Martina C. Schwerzmann[1,2]
Valerie G. A. Suter[1]
Thomas von Arx[1]

[1] Department of Oral Surgery and Stomatology, School of Dental Medicine, University of Bern, Switzerland
[2] Clinic for Cranio-Maxillofacial Surgery, University Hospital of Zurich, Department of Oral and Maxillofacial Surgery, Zurich, Switzerland

CORRESPONDENCE
Dr. med. dent.
Martina C. Schwerzmann
Klinik für Mund-, Kiefer- und Gesichtschirurgie
Universitätsspital Zürich
Rämistrasse 100
CH-8091 Zürich
Tel. +41 44 255 81 33
E-mail:
martina.schwerzmann@usz.ch

SWISS DENTAL JOURNAL SSO 132: 10–17 (2022)
Accepted for publication:
9 June 2020

The anatomical variability of the sphenoid sinus in CBCT

A retrospective study

KEYWORDS
Sphenoid sinus
Anatomical variations
Cone-beam computed tomography (CBCT)
Pattern of septation

SUMMARY
The aim of this retrospective study was to assess and illustrate the anatomical variability of the sphenoid sinus (SPS) on cone-beam computed tomography (CBCT) scans. A total of 50 SPS were assessed. CBCT images were oriented in the sagittal plane to evaluate the type of pneumatization (conchal, presellar, sellar and postsellar). Size measurements (width, length and height) of the SPS as well as the septation pattern and the presence or absence of pathologies were examined in all three planes. The postsellar type (28 cases, 56%) was the most common pattern of pneumatization. Conchal, presellar, or sellar pneumatization were significantly less frequent. There was only one case (2%) with a conchal and two cases (4%) with a presellar type. Multiple septa were found in 75% of patients with postsellar pneumatization, but only in 45.5% of patients featuring conchal, presellar or sellar types. In the postsellar category, all measured dimensions were significantly higher compared to the other types of pneumatization. Pathologies in the SPS were found in 7 patients (14%). It was concluded that the anatomical structure of the SPS is highly variable. Knowledge about its radiological appearance in CBCT will help in identification of pathologies and surrounding anatomical structures.

Introduction

The sphenoid sinus (SPS) is the most posterior and the most variable of the paranasal sinuses in size and shape (Budu et al. 2013; Anusha et al. 2014; von Arx et al. 2020). It is located within the central body of the sphenoid bone (Fig. 1). The sphenoid bone itself is a complex structure of the cranium containing a central body, paired lesser and greater wings as well as pterygoid processes. The superior part of the sphenoid bone forms the superior wall of the SPS and contributes to the anterior and middle fossae of the skull base (Budu et al. 2013). A bony depression impresses as the sella turcica and serves as a fossa for the pituitary gland (von Arx et al. 2020). Anteriorly, the superior part of the sphenoid bone extends into the roof of the ethmoid sinus. The anterior wall of the SPS is connected to the vomer in the midline and to the perpendicular plate of the ethmoid (Budu et al. 2013). The sinus ostia are located in the anterior wall of the SPS. As shown in Figure 2, the drainage takes place via the sphenoethmoidal recess into the superior meatus (von Arx et al. 2020). Because of its anatomical location and difficult accessibility, the SPS had been poorly examined until the advent of endoscopes and modern imaging techniques including computed tomography (CT) and later cone-beam computed tomography (CBCT) (Anusha et al. 2014). In fact, CBCT has become a standard of care for radiographic assessment of complex cases and treatment planning in dental medicine (Bornstein et al. 2014). In the diagnostic assessment of the paranasal sinuses, CBCT is increasingly applied as an alternative to CT (Demiralp et al. 2018). Despite the complex anatomy, the SPS is the least examined among the paranasal sinuses. Studies assessing morphologic variations of the SPS and its related structures are limited (Princip et al. 2019; Yalcin 2020).

Complex anatomical structures such as the retromaxillary region including the SPS, which the general dentist is usually not familiar with, become visible in CBCT (von Arx et al. 2020). However, the entire volume of the acquired data set needs to be analyzed according to the European Commission's Evidence Based Guidelines (European Commission 2012; Pauwels 2015). Using a series of 50 selected cases, this paper reviews and highlights the complex anatomical structure of the SPS as well as its identification and interpretation using CBCT.

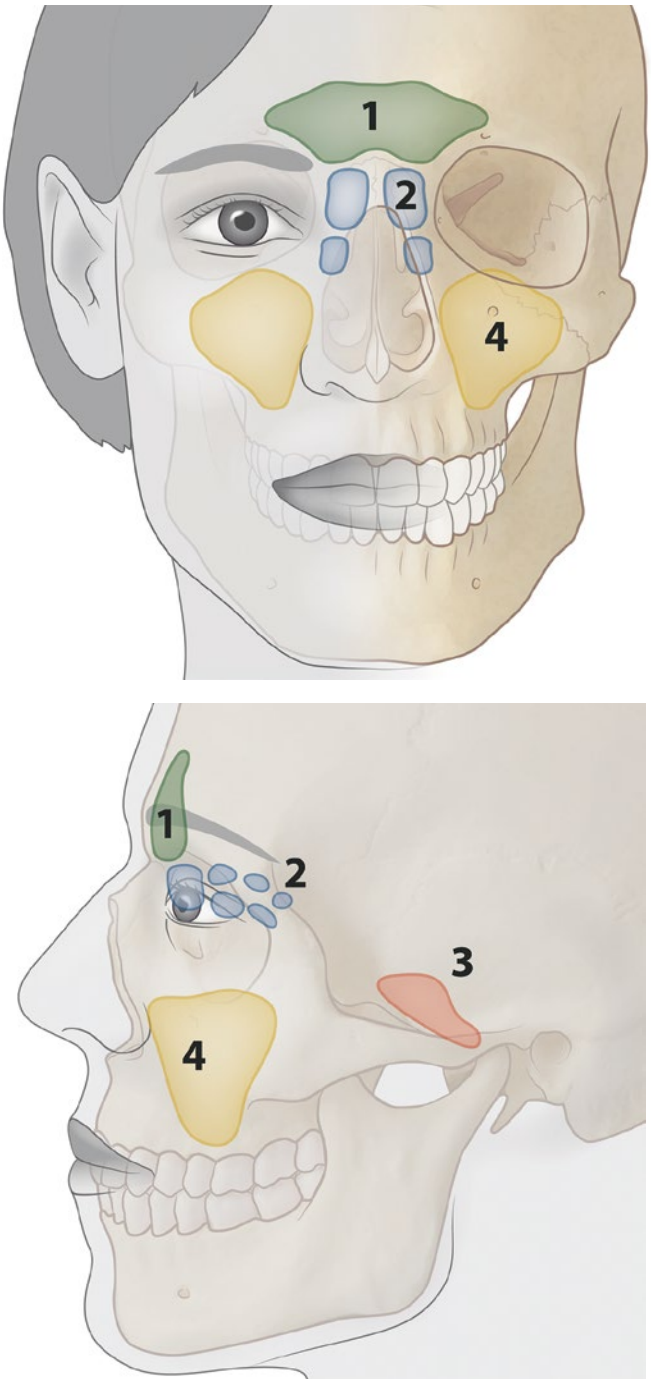

Fig. 1 Schematic illustration of the paranasal sinuses: 1 = frontal sinus; 2 = ethmoid sinus; 3 = sphenoid sinus; 4 = maxillary sinus

Materials and methods

Patient selection

CBCTs from patients who underwent radiologic assessment between 2010 and 2020 at the section of Dental Radiology and Stomatology, Department of Oral Surgery and Stomatology, University of Bern, were eligible, provided the SPS was completely visible in all dimensions. Patients were either in-house or had been referred. The growth of the sphenoid sinus is completed by the end of puberty (Budu et al. 2013). Therefore, patients younger than 18 years of age were excluded. Furthermore, a partially visible SPS was considered an exclusion criterion. A total of 50 CBCTs were included for the final examination. The local ethics committee of the canton of Bern, Switzerland, approved the study protocol (approval number: KEK-BE 2020-01589).

Radiographic assessment

All CBCT images were recorded with a 3D Accuitomo 170 unit (J Morita Corp., Kyoto, Japan) in a sitting position and with the head fixed, centered in the middle of the face, and aligned horizontally to the Frankfurt plane (lower border of orbita to tragion). The exposure parameters were 5–7 mA and 90 kV, and the exposure time was 17.5 seconds with a full scan rotation (360°) in all cases. Only one case had a different exposure time of 9.0 seconds and a half scan rotation (180°). The different field of views included 10 × 10 cm, 14 × 10 cm and 17 × 12 cm with a voxel size of 0.25 mm. The devices were operated by a team that is well experienced in dentomaxillofacial radiology. All measurements were made with tools of the corresponding software (i-Dixel, version 2.2.1.2., J Morita Corp., Kyoto, Japan).

A calibrated observer (M.S.) performed the measurements once on a Dell 380 precision work station (Dell SA, Geneva, Switzerland) and a 19-inch EIZO FlexScan monitor with a reso-

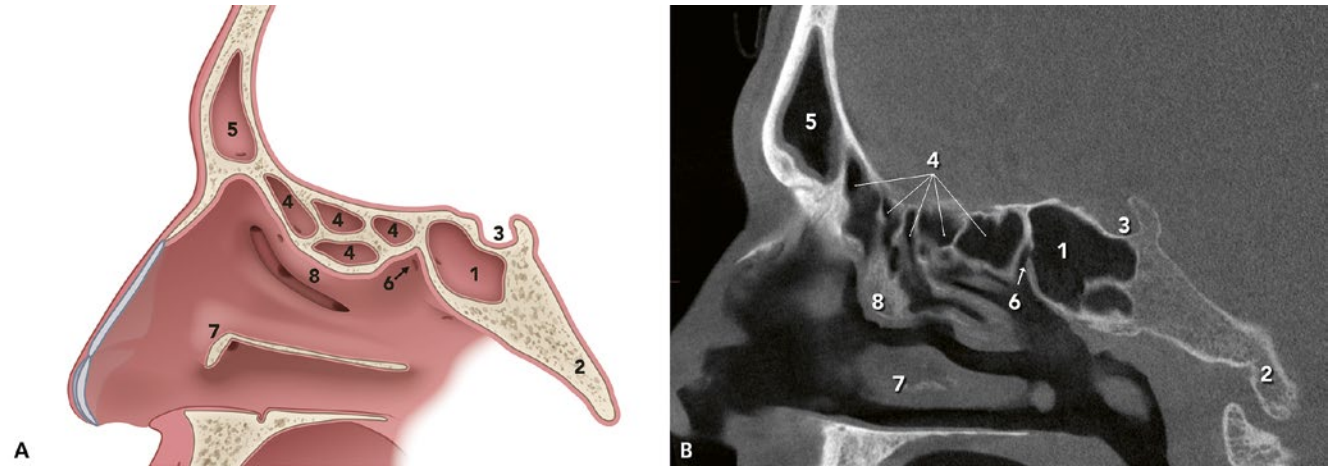

Fig. 2 Schematic illustration (A) and CBCT image (B) of the SPS and adjacent structures (sagittal view): 1 = sphenoid sinus; 2 = clivus (occipital bone); 3 = sella turcica; 4 = ethmoid cells (ethmoid sinus); 5 = frontal sinus; 6 = sphenoethmoidal recess with opening of sphenoid sinus; 7 = partially resected inferior concha; 8 = bulla ethmoidalis

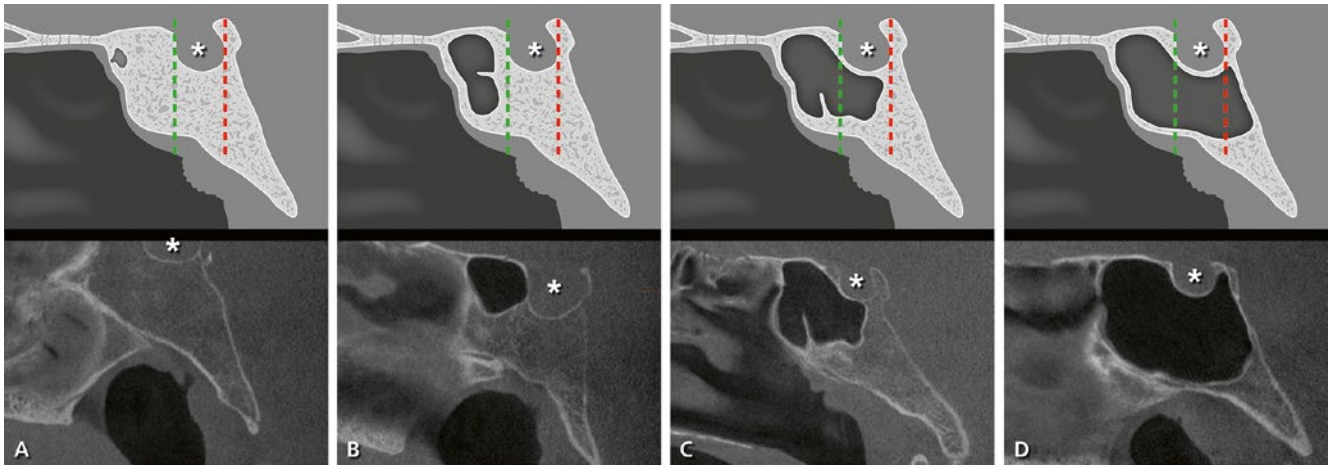

Fig. 3 Schematic illustration and CBCT sections through the SPS of four different patients showing the different types of extension of the SPS according to the relationship with the sella turcica (sagittal view): A = conchal type; B = presellar type; C = sellar type; D = postsellar type; * = sella turcica; green line = vertical line drawn through the tuberculum sellae; red line = vertical line drawn through the posterior margin of the sella turcica

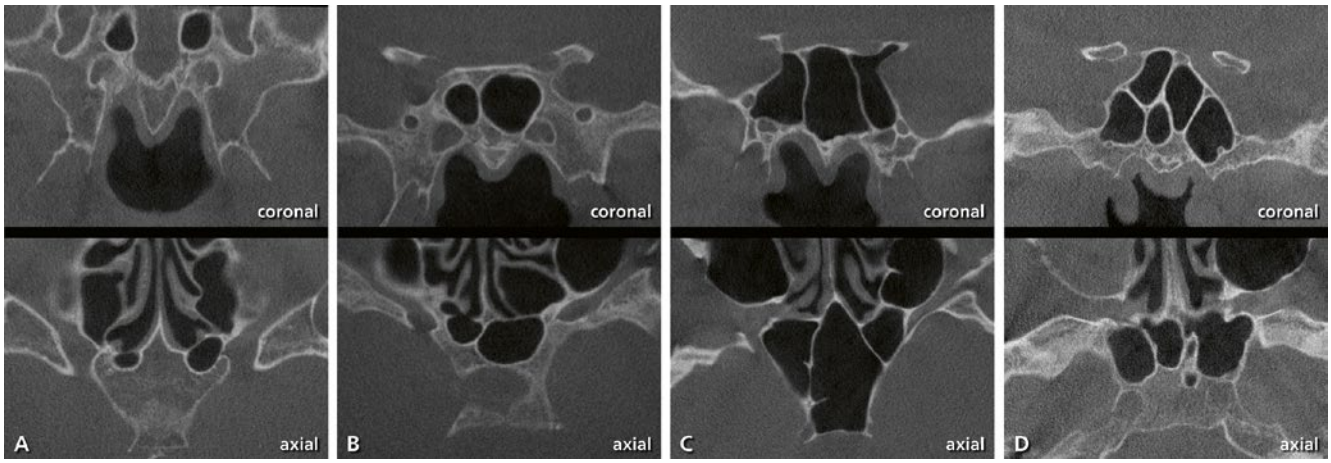

Fig. 4 CBCT sections of varying number and appearance of septa in four different patients (coronal und axial views): A = two separate chambers with no septum; B = one septum; C = two septa; D = multiple septa

lution of 1,280 × 1,024 pixels (Eizo Nanao AG, Wädenswil, Switzerland). The study parameters were assessed in all three individually adapted planes (sagittal, coronal, axial). The height was measured in the sagittal and coronal plane from the most caudal point of the SPS to the floor of the anterior and middle cranial fossae. The landmark determination for the measurement of the length was the most anterior and the posterior part of the bony wall of the SPS, examined in sagittal and axial planes. The central wall of the greater and lesser wings was determined as landmarks for the measurement of the width in the coronal and

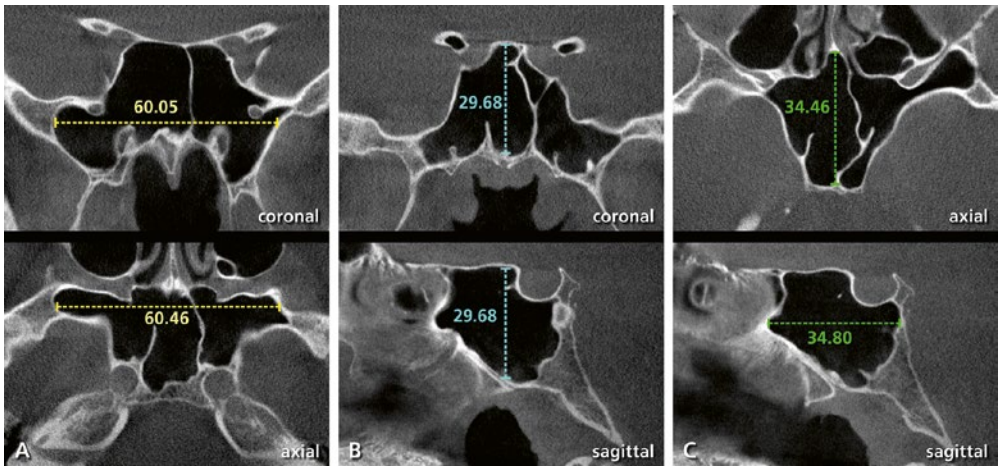

Fig. 5 Size measurements of the SPS in CBCT of a 22-year-old male: A = width in the coronal and axial planes; B = height in the coronal and sagittal planes; C = length in the axial and sagittal planes

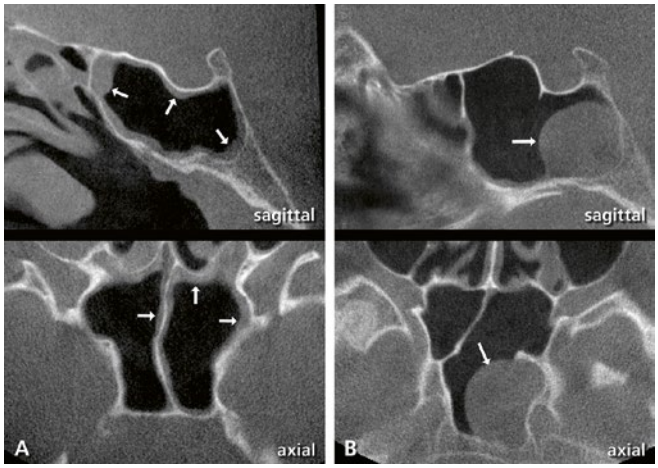

Fig. 6 CBCT images with pathologies inside the SPS (sagittal und axial views): A = mucosal thickening; B = mucous retention cyst

axial planes. The type of pneumatization was assessed in the sagittal plane. The pattern of septation was examined in the coronal and axial planes.

The following parameters were analyzed:

A: sinus pneumatization type evaluated on sagittal plane images (Fig. 3)

B: number and appearance of septa (intersphenoid or accessory) in all three planes (Fig. 4)

C: size measurements (width, height, length) in all three planes (Fig. 5)

D: presence/absence of pathologies in all three planes (Fig. 6)

Statistical analysis

Statistical analysis was performed with open source software R, Version 4.0.2 (R Core Development Team 2019). To assess differences of SPS dimensions (width, length, height) as well as differences between the number of septa types (intersphenoid vs. accessory), exact Mann-Whitney tests were performed. For these outcomes, descriptive statistics were calculated in the form of medians and ranges. To assess differences in categorical parameters, exact Fisher tests for 2 × 2 contingency tables were performed along with odds ratios including a 95% confidence interval. Throughout, p-values less than 0.05 were considered as statistically significant. No correction for multiple testing was applied as no post hoc tests were performed.

Results

This retrospective study evaluated a total of 50 CBCTs depicting the complete SPS. 26 patients (52%) were male and 24 (48%) female. Regarding age, 32% of the patients were younger than 45 years and 68% of patients were older (range 18–90, median 53.4). The median width, length and height were slightly larger in the male group. However, this difference was not significant. Age had no significant influence on length, width and height of the SPS (Tab. I).

Regarding the degree of pneumatization of the SPS, there was only one case with a conchal type and two cases with a presellar type. The frequency of the postsellar type was 56% (28 patients), while the three other types were found in the remaining 22 cases. In the postsellar type, significantly higher dimension values were found compared with the group of conchal, presellar and sellar types (width and length: $p < 0.0004$, height: $p < 0.0003$). The median width of the postsellar SPS was 39.9 mm, the median length 32.0 mm and the median height 26.3 mm. In the group of conchal, presellar and sellar pneumatizations, a median width of 30.1 mm, a median length of 21.2 mm and a median height of 23.5 mm was found (Tab. II).

Patients with a postsellar pneumatization had significantly higher odds of presenting multiple septa (OR: 3.5, $p = 0.043$): 75% (21 patients) with a postsellar type had multiple septa (Tab. III). Overall, 8 patients (16%) had only one intersphenoid septum without accessory septa. 10 patients (20%) had two septa. Only the patient with the conchal type of pneumatization had no septum. Width was significantly wider in patients with multiple septa (Tab. IV) and the number of accessory septa was significantly higher in patients with multiple septa (Tab. V).

In 7 patients (14%), a pathological condition inside the SPS was observed. The pathologies were interpreted as mucosal thickening in 4 and as mucous retentions cysts in 3 cases.

Discussion

CBCT enables improved diagnostics and thus more predictable planning of the interventions in dentistry. For this reason, an increasing use of CBCT can be observed (Pauwels 2015). According to the European Commission's Evidence Based Guidelines,

Tab. I Influence of possible factors on the dimension of the sphenoid sinus

				Width [mm]			Length [mm]			Height [mm]		
Parameter	**Subcategory**	**N**	**%**	**Median**	**Range**	**P value**	**Median**	**Range**	**P value**	**Median**	**Range**	**P value**
Sex	Male	26	52	36.8	22.3–60.3	0.78	31.1	12.3–38.5	0.11	25.6	12.0–34.0	0.19
	Female	24	48	33.1	6.8–66.5		28.0	6.8–35.4		24.3	7.8–27.8	
Age	< 45 years	16	32	39.7	23.3–60.3	0.29	30.8	15.9–38.5	0.12	25.8	17.4–34.0	0.14
	≥ 45 years	34	68	34.2	6.8–66.5		28.0	6.8–37.0		24.3	7.8–30.3	

Tab. II Influence of the dimensions on the type of pneumatization of the sphenoid sinus

				Width [mm]			Length [mm]			Height [mm]		
Parameter	**Subcategory**	**N**	**%**	**Median**	**Range**	**P value**	**Median**	**Range**	**P value**	**Median**	**Range**	**P value**
Type of pneumatization	Conchal/presellar/sellar	22	44	30.1	6.8–49.0	$< 10^{-4}$	21.2	6.8–29.5	$< 10^{-4}$	23.5	7.8–34.0	3×10^{-3}
	Postsellar	28	56	39.9	26.8–66.5		32.0	25.6–38.5		26.3	21.0–30.3	

Tab. III Influence of the pneumatization of the sphenoid sinus on the number of septa

				0–2 septa		Multiple septa		Statistics	
Parameter	**Subcategory**	**N**	**%**	**N**	**%**	**N**	**%**	**P value**	**Odds ratio**
Type of pneumatization	Conchal/presellar/sellar	22	44	12	54.5	10	45.5	0.043	3.5 (1.0–14.2)
	Postsellar	28	56	7	25.0	21	75.0		

Tab. IV Influence of the dimensions on the number of septa and the septation pattern of the sphenoid sinus

				Width [mm]			Length [mm]			Height [mm]		
Parameter	**Subcategory**	**N**	**%**	**Median**	**Range**	**P value**	**Median**	**Range**	**P value**	**Median**	**Range**	**P value**
Septation pattern	0–2 septa	19	38	30.7	6.8–42.7	3×10^{-3}	24.0	6.8–36.6	0.06	23.8	7.8–34.0	0.25
	Multiple septa	31	62	39.1	25.7–66.5		29.3	15.8–38.5		24.9	17.3–29.7	

Tab. V Influence of the number of septa on the kind of septa

				Intersphenoid septa		Accessory septa		Statistics
Parameter	**Subcategory**	**N**	**%**	**Median**	**Range**	**Median**	**Range**	**P value intersphenoid septa vs. accessory septa**
Septation pattern	0–2 septa	19	38	1	1–2	0	0–1	3×10^{-4}
	Multiple septa	31	62	1	1–1	2	1–5	$< 10^{-4}$

the practitioner should evaluate the entire volume and they need to be able to recognize possible pathologies or incidental findings and not just the region of interest (European Commission 2012; Pauwels 2015). Thus, even if not directly influencing the dental intervention, the SPS including its variable size and shape should be recognized by a dentist using CBCT.

Pneumatization of the sphenoid sinus and dimensions

In line with other studies, the most common types of pneumatization were the sellar and postsellar types while the postsellar type was the sinus with the largest dimensions (Sareen et al. 2005; Hamdi et al. 2008; Bude et al. 2013; Anusha et al. 2014; Wiebracht et al. 2014; Štoković et al. 2016). There is no typical appearance of the SPS. The less common variants must therefore be recognized and not misinterpreted as pathology. The great variability of the SPS is directly related to the variability of pneumatization. Most authors prefer the Hammer and Radberg classification of SPS extension including three types based on the location of the posterior sinus wall with respect to the sella turcica (Hammer et al. 1961; Anusha et al. 2014; von Arx et al. 2020). The conchal (or fetal) type represents a very small sinus or pneumatization is completely absent (agenesis) and the "sinus" is filled with cancellous bone (Wiebracht et al. 2014; Duman et al. 2020). The presellar (or juvenile) type has pneumatization extending to the sella turcica. The posterior sinus border remains anterior to a vertical line drawn through the tuberculum sellae while the sellar (or adult) type extends beyond this vertical line. Hamid et al. (2008) divided the Hammer and Radberg classification of sellar types into two subcategories: sellar and postsellar, divided by a vertical line drawn through the posterior margin of the sella (Fig. 3). The most frequent type of pneumatization is the postsellar type, followed by the sellar and the presellar types. The conchal type is rare and found in 2% (Budu et al. 2013). These data as well as those from CT and magnetic resonance imaging (MRI) studies (Hamid et al. 2008) and CBCT/cadaveric studies (Štoković et al. 2016) largely coincide with the results of the present study. Patients having a postsellar type showed higher values in all three dimensions than patients with conchal, presellar und sellar types. A correlation with male gender and age was found in other studies, which is in contrast to the present findings (Sareen et al. 2005; Cohen et al. 2018). Differences in measurement techniques or alterations of head positions during CBCT scanning could be a possible explanation of variable results. According to El-Beialy et al. (2011) and Adibi et al. (2017) slight variations in the skull orientation should not affect the accuracy and reliability of the measurements.

Pattern of septation

The SPS is commonly separated into two asymmetrical cavities by an intervening bony septum. This septum is often deviated laterally to the midsagittal plane and creates a "dominant" sinus (Sareen et al. 2005; An & Ong 2007; Budu et al. 2013; Anusha et al. 2014; von Arx et al. 2020). Frequently, more than one septum can be observed resulting in complex sinus subdivisions. The cadaveric study by Sareen et al. (2005) found multiple intersinus septa in 80% of the cases which is similar to the data (73%) of an earlier cadaveric and radiological study by Elwany et al. (1983). In contrast, Hamid et al. (2008) observed only 6.8% multiple septa in their large CT and MRI study. Besides the number of septa, the anatomical site of attachment of the septa is clinically relevant (Wiebracht et al. 2014). Hence, accessory septa are subdivisions that do not form closed chambers within the SPS. In 31 patients (62%), multiple septa were found. In these cases, the range of accessory septa was 1–5 (Tab. V). Patients with 0–2 septa had more intersphenoid septa than accessory septa (median: 1 vs. 0, $p = 0.003$). The contrary is true for patients with multiple septa (median: 1 vs. 2, $p < 0.0001$) (Tab. V). In addition, a significantly larger width ($p < 0.0003$) of the SPS was found when multiple septa were present (Tab. IV).

Pathologies

Pathologies within the SPS are generally rare: infections and/or inflammations are the most common, either a bacterial or a fungal sphenoiditis (Fooanant et al. 2017). Sphenoid sinus opacification on imaging is a typical radiological finding due to infections. Unilateral opacification may indicate a neoplasia (Knisely et al. 2017). In fact, the second most frequent pathology of the SPS is a tumor, malignant in 7% of the cases (Fooanant et al. 2017). The diagnosis is challenging because patients are often asymptomatic or present atypical symptoms (Beton et al. 2016). Compared to the other paranasal sinuses, the SPS is usually not affected with rhinorrhea or nasal congestion. Headache, often hemicranial, may occur with sphenoiditis or be associated with a tumor (Fooanant et al. 2017). Another possible symptom is visual alteration such as diplopia or reduced visual acuity, more frequently associated with tumors than sphenoiditis. Because physical examination of the SPS is difficult due to its deep location within the skull, imaging plays an important role (Knisely et al. 2017). MRI and CT are the most helpful and used tools for imaging sinus pathologies (Beton et al. 2016). But, pathologies related to the SPS can be found in large field of views in CBCT and may be challenging to interpret correctly. In the present study, pathologies in the SPS were found in 7 of the 50 patients (14%). While in 4 patients the indication for the CBCT was the suspicion of maxillary sinusitis or pansinusitis, the pathologies in the other 3 patients were considered as incidental findings. Only in one patient the final diagnosis and the subsequent therapy were known. The radiologically confirmed pansinusitis was treated with antibiotics. Reviewing the entire volume of the CBCT is therefore a necessity. In case of a neoplastic process, a delayed diagnosis may lead to serious complications (Beton et al. 2016).

Conclusion

With regard to the findings of the present retrospective CBCT study, it can be concluded that the SPS is a highly variable anatomical structure. The sellar and postsellar pneumatization types predominate compared to the rarely found presellar or conchal types. Knowledge about the anatomical structures of the SPS can help with the overall evaluation of CBCTs and are necessary to identify possible pathologies, found in 14% in the present study.

Acknowledgement

The authors are grateful to Bernadette Rawyler, Medical Illustrator, and Ines Badertscher, Media Designer, School of Dental Medicine, University of Bern, Bern, Switzerland, for the illustrations and preparation of the figures. We also would like to thank Dr. Lukas Martig, significantis GmbH, Bern, Switzerland, for the statistical analysis.

Conflict of interest / financial disclosures

The authors declare that there are no conflicts of interest related to this manuscript. The authors have nothing to disclose.

Zusammenfassung

Einleitung

In dieser Arbeit wird die Anatomie der Keilbeinhöhle *(Sinus sphenoidalis)* in der digitalen Volumentomografie (DVT) untersucht. Diese Struktur wird bei grösseren Volumina auf dem DVT-Bild häufig partiell am Rand des Fensters abgebildet oder seltener auch vollständig dargestellt. Von allen Nasennebenhöhlen ist der *Sinus sphenoidalis* die anatomisch variabelste und liegt am weitesten posterior. Gebildet wird sie vom zentralen Anteil des unpaaren Keilbeins *(Os sphenoidale)*, das in seiner Form einem Schmetterling gleicht und zentral im Schädelskelett liegt. Die hochvariable Ausdehnung der Keilbeinhöhle wird unter anderem anhand von Pneumatisationstypen *(conchal, presellar, sellar* und *postsellar)* beschrieben und ist abhängig von der Beziehung zur *Sella turcica.* In den meisten Fällen zeigt sich der *Sinus sphenoidalis* als paarige Struktur mit einem durchgängigen intersphenoidalen Septum. Häufig sind aber auch multiple Septen vorhanden, wobei sich diese als akzessorische Teilsepten oder als zusätzliches intersphenoidales Septum präsentieren. Pathologien im *Sinus sphenoidalis* führen selten zu Beschwerden, sind aber gelegentlich auf dem DVT-Bild als Zufallsbefund zu erkennen.

Material und Methoden

In dieser retrospektiven Studie wurden die DVT-Bilder von 50 Patienten im Alter zwischen 18 und 90 Jahren ausgewertet, die zwischen 2010 und 2020 an der Klinik für Oralchirurgie und Stomatologie der Universität Bern erstellt wurden. In der Sagittalebene wurde der Pneumatisationstyp bestimmt. Die Vermessung des *Sinus sphenoidalis* (Breite, Länge, Höhe) sowie die Beurteilung des Septenmusters (Anzahl und Art der Septen) erfolgte in allen drei Ebenen. Ebenfalls wurden die DVT-Bilder nach allfälligen Pathologien im *Sinus sphenoidalis* untersucht.

Resultate

Wie bereits in früheren Studien gezeigt, stellen der sellare und der postsellare Typ die weitaus häufigsten Formen dar. Der conchale Typ konnte nur bei einem Patienten (2%) beobachtet werden. Das Septenmuster präsentierte sich sehr variabel. In dieser Arbeit konnte ein signifikanter Zusammenhang zwischen Pneumatisationstyp und Septenanzahl aufgezeigt werden, wobei der postsellare Pneumatisationstyp in 75% multiple Septen aufwies und die anderen Pneumatisationstypen nur in 45,5% (OR 3,5, $p = 0{,}043$). Die Dimensionen (Breite, Länge und Höhe) variierten stark (vgl. Ranges in allen Gruppen; Tab. I und II), sind aber beim postsellaren Typ signifikant grösser als bei den anderen Pneumatisationstypen ($p < 0{,}0001$ bezüglich Breite und Länge des SPS, $p = 3 \times 10^{-3}$ bezüglich Höhe, Tab. II). Pathologien konnten in 14% (7 Patienten) gefunden werden, wobei es sich entweder um Schleimretentionszysten oder Schleimhautverdickungen handelte.

Diskussion

Die Resultate und die statistische Auswertung dieser Arbeit bestätigen die anatomische Vielfalt anhand der unterschiedlichen Pneumatisationstypen und der variablen Septenmuster sowie der grossen Dimensionsunterschiede. Ein Basiswissen über die untersuchten Parameter ermöglicht eine korrekte Identifikation des *Sinus sphenoidalis.* Die Lokalisation der Keilbeinhöhle wiederum kann bei der Orientierung und der Gesamtbeurteilung des DVT-Bilds hilfreich sein. Bei grossen Fenstern, in denen Oberkiefer und Mittelgesicht im *field of view* zu sehen sind, besteht eine relativ hohe Wahrscheinlichkeit, dass auch der *Sinus sphenoidalis* teilweise abgebildet wird. Die vollständige Abbildung dieser anatomischen Struktur ist hingegen eher selten. Gemäss den European Commissions's of Evidence Based Guidelines (European Commission 2012) muss das gesamte Datenvolumen eines DVT-Bilds beurteilt werden. Aus diesem Grund sind Kenntnisse über die der *region of interest* angrenzenden Regionen zwingend und für die Erkennung von allfälligen Pathologien unabdinglich.

Résumé

Introduction

Dans ce travail, l'anatomie du sinus sphénoïdal *(Sinus sphenoidalis)* est examinée au cone beam CT (CBCT). Dans un CBCT de grand volume, cette structure anatomique est souvent représentée au bord du champ d'acquisition et, plus rarement, elle est complètement représentée. Parmi tous les sinus paranasaux, le sinus sphénoïdal est celui qui est le plus variable anatomiquement et celui qui est situé le plus postérieur. Il est situé dans la partie centrale de l'os sphénoïdal impair *(Os sphenoidale)* qui a une forme qui ressemble à un papillon et qui se trouve au milieu du squelette crânien. L'extension du sinus sphénoïdal est en rapport avec le type de pneumatisation *(conchale, présellaire, sellaire et postsellaire)* et dépend aussi de la relation avec la *sella turcica.* Dans la plupart des cas, le sinus sphénoïdal est une structure appariée et présente un septum intersphénoïdal continu. Souvent, il y a plusieurs septa qui sont partiels accessoires ou il y a un septum intersphénoïdal supplémentaire. Les pathologies du sinus sphénoïdal sont rarement liées à des symptômes, mais peuvent parfois être une découverte fortuite en imagerie CBCT.

Matériel et méthodes

Dans cette étude rétrospective, les images CBCT de 50 patients âgés de 18 à 90 ans, prises entre 2010 et 2020 à la Clinique de chirurgie orale et de stomatologie de l'Université de Berne, ont été évaluées. Le type de pneumatisation a été déterminé dans le plan sagittal. La mesure du *Sinus sphenoidalis* (largeur, longueur, hauteur) et la configuration des septa (nombre et type de septa) ont été effectuées dans les trois plans (sagittal, coronal, axial). Les images CBCT ont également été examinées pour l'identification d'éventuelles pathologies dans le sinus sphénoïdal.

Résultats

Comme dans d'autres études publiées précédemment, le sinus sphénoïdal de type sellaire et postsellaire était la forme la plus courante. Le type conchal n'a pu être observé que chez un seul patient (2%). La configuration et le nombre de septa étaient très variables. Dans ce travail, une relation significative entre le type de pneumatisation et le nombre de septa a pu être mise en évidence. C'est le type postsellaire qui a été le plus souvent observé avec de multiples septa, trouvés chez 75% des patients avec ce type de sinus (OR 3,5, $p = 0{,}043$). Les dimensions (largeur, longueur et hauteur) du sinus sphénoïdal variaient considérablement (voir variations dans tous les groupes; tab. I et II), mais étaient nettement plus grandes pour le type postsellaire que pour les autres types de pneumatisation ($p < 0{,}0001$ pour la largeur et la longueur, $p = 3 \times 10{-}3$ pour la hauteur, tab. II).

Des pathologies ont été identifiées chez 14% (7 patients). Il s'agissait soit de kystes de rétention muqueux, soit d'un épaississement de la muqueuse.

Discussion

Les résultats et l'analyse statistique de ce travail confirment la diversité anatomique des différents types de pneumatisation et la variabilité des septa ainsi que les grandes différences de dimensions du sinus sphénoïdal. La connaissance des paramètres présentés dans ce travail aide à identifier et interpréter correctement le sinus sphénoïdal lors de l'évaluation radiologique. Localiser le sinus sphénoïdal peut être utile pour orienter le CBCT et pour procéder à son évaluation générale. Lors de la prise d'un CBCT de grand volume qui inclut la mâchoire supérieure et le tiers moyen de la face, il existe une probabilité relativement élevée que le sinus sphénoïdal soit partiellement ou, plus rarement, totalement représenté. Selon les recommandations de radioprotection en radiologie CBCT maxillofaciale, publiées comme « European Commission evidence-based guidelines » (European Comission 2012), le volume total du CBCT doit être évalué. Cela signifie que la connaissance de l'anatomie de la région avoisinante à la région de l'intérêt est essentielle pour la détection d'éventuelles pathologies.

References

Adibi S, Shahidi S, Nikanjam S, Paknahad M, Ranjbar M: Influence of head position on the CBCT accuracy in assessment of the proximity of the root apices to the inferior alveolar canal. J Dent 18: 181–186 (2017)

Anusha B, Baharudin A, Philip R, Harvinder S, Shaffie B M: Anatomical variations of the sphenoid sinus and its adjacent structures: A review of existing literature. Surg Radiol Anat 36: 419–427 (2014)

Beton S, Basak H, Ocak E, Kucuk B, Yorulmaz I, Meco C: How often does isolated sphenoid sinus disease turn out to be a neoplasm? J Craniofac Surg 27: 41–43 (2016)

Bornstein M M, Scarfe W C, Vaughn V M, Jacobs R: Cone beam computed tomography in implant dentistry: a systematic review focusing on guidelines, indications, and radiation dose risks. Int J Oral Maxillofac Implants 29: 55–77 (2014)

Budu V, Mogoanta C A, Fanuta B, Bulescu I: The anatomical relations of the sphenoid sinus and their implications in sphenoid endoscopic surgery. Rom J Morphol Embryol 54: 13–16 (2013)

Cohen O, Warman M, Fried M, Shoffel-Havakuk H, Adi M, Halperin D, Lahav Y: Volumetric analysis of the maxillary, sphenoid and frontal sinuses: A comparative computerized tomography based study. Auris Nasus Larynx 45: 96–102 (2018)

Demiralp K O, Cakmak S K, Aksoy, Bayrak S, Orhan K, Demir P: Assessment of paranasal sinus parameters according to ancient skulls' gender and age by using cone-beam computed tomography. Folia Morphol 78: 344–350 (2019)

Duman S B, Dedeoglu N, Arikan B, Altun O: Sphenoid sinus agenesis and sella turcica hypoplasia: very rare cases of two brothers with Hamamy syndrome. Surg Radiol Anat 42: 1377–1380 (2020)

El-Beialy A R, Fayed M S, El-Bialy A M, Mostafa Y A: Accuracy and reliability of cone-beam computed tomography measurements: Influence of head orientation. Am J Orthod Dentofac Orthop 140: 157–165 (2011)

Elwany S, Yacout Y M, Talaat M, El-Nahass M, Gunied A, Talaat M: Surgical anatomy of the sphenoid sinus. J Laryngol Otol 97: 227–241 (1983)

European Commission: Radiation Protection no 172, Cone beam ct for dental and maxillofacial radiology. Evidence-Based Guidelines (2012)

Fooanant S, Angkurawaranon S, Angkurawaranon C, Roongrotwattanasiri K, Chaiyasate S: Sphenoid Sinus Diseases: A Review of 1,442 Patients. Int J Otolaryngol 2017: 1–7 (2017)

Hamid O, El Fiky L, Hassan O, Kotb A, El Fiky S: Anatomic variations of the sphenoid sinus and their impact on transsphenoid pituitary surgery. Skull Base 18: 9–15 (2008)

Hammer G, Radberg C: The sphenoidal sinus. An anatomical and roentgenologic study with reference to transsphenoid hypophysectomy. Acta radiol 56: 401–422 (1961)

Jaju P P, Jaju S P: Cone-beam computed tomography: Time to move from ALARA to ALADA. Imaging Sci Dent 45: 263–265 (2015)

Knisely A, Holmes T, Barham H, Sacks R, Harvey R: Isolated sphenoid sinus opacification: A systematic review. Am J Otolaryngol 38: 237–243 (2017)

Pauwels R: Cone beam CT for dental and maxillofacial imaging: Dose matters. Radiat Prot Dosimetry 165: 156–161 (2015)

Pauwels R, Araki K, Siewerdsen J H, Thongvigitmanee S S: Technical aspects of dental CBCT: State of the art. Dentomaxillofacial Radiol 44: 1–20 (2015)

Pirinc B, Fazliogullari Z, Guler I, Unver N, Ismihan D, Uysal I: Classification and volumetric study of the sphenoid sinus on MDCT images. Eur Arch Oto-Rhino-Laryngology 76: 2887–2894 (2019)

R Core Development Team: R: A language and environment for statistical computing. Vienna, Austria (2019)

Sareen D, Agarwal A K, Kaul J M, Sethi A: Study of Sphenoid Sinus Anatomy in Relation to Endoscopic Surgery. Int J Morphol: 23 (2005)

Štoković N, Trkulja V, Dumić-Čule I, Čuković-Bagić I, Lauc T, Vukičević S, Grgurević L: Sphenoid sinus types, dimensions and relationship with surrounding structures. Ann Anat 203: 69–76 (2016)

Tan H K, Ong Y K: Sphenoid sinus: An anatomic and endoscopic study in Asian cadavers. Clin Anat 20: 745–750 (2007)

von Arx T, Lozanoff S, Bornstein M M: Extraoral anatomy in CBCT – a literature review. Part 2: Zygomatico-orbital region. Swiss Dent J 130: 126–138 (2020)

Wiebracht N D, Zimmer L A: Complex Anatomy of the Sphenoid Sinus: A Radiographic Study and Literature Review. J Neurol Surgery, Part B Skull Base 75: 378–382 (2014)

Yalcin E D: Assessment of sphenoid sinus types in patients with cleft lip and palate on cone-beam CT. Eur Arch Oto-Rhino-Laryngology 277: 1101–1108 (2020)